Original Article: Open Access

VIBGYOR ePress

International Journal of
Metallurgy and Metal Physics

Corrosion Behavior of Mechanically Alloyed SUS304L with Zirconium Addition in High-Temperature Water

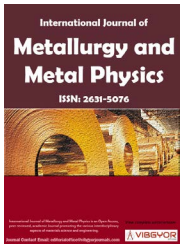

ISSN: 2631-5076

Daniel Morrall[1*], Yen-Jui Huang[2], Kiyohiro Yabuuchi[2], Akihiko Kimura[2], Takahiro Ishizaki[3] and Yusaku Maruno[3]

[1]*Graduate School of Energy Science, Kyoto University, Japan*

[2]*Institute of Advanced Energy, Kyoto University, Japan*

[3]*Research & Development Group, Hitachi Ltd., Japan*

Abstract

A mechanically alloyed austenitic stainless steel (MA304LZ) was produced from pre-alloyed SUS304L powder with a small amount of zirconium addition. Coupon-type specimens of MA304LZ and SUS304L steels were subjected to hot water at 300 °C/25 MPa and supercritical pressurized water (SCW) at 500 °C/25 MPa for 1000 hr. MA304LZ is significantly less susceptible to corrosion weight gain in SCW than SUS304L which follows the parabolic rule between weight gain and elapsing time. The reduction of weight gain in MA304LZ can be attributed to much smaller grains which enhance chromium diffusion through grain boundaries and consequently accelerate the formation of a protective chromium oxide layer. Nickel oxides were observed in SUS304L but not in MA304LZ after the test at 500 °C. It is considered that zirconium addition suppresses nickel diffusion as well as oxygen diffusion because of the strong interaction of zirconium/nickel and zirconium/oxygen. Electrochemical potentiodynamic reactivation (EPR) measurement of the degree of sensitization (DOS) of annealed and non-annealed samples indicates that both steels were resistant to sensitization of grain boundary corrosion. However, the annealing of MA304LZ at 1050 °C diminishes the beneficial grain size effect of MA304LZ.

Keywords

Mechanical alloying, Fine grains, Zr addition, Corrosion, Supercritical water

Introduction

Enhancing the safe operation of nuclear reactors with use of advanced materials is of upmost importance for meeting future energy demands including a reduction of carbon dioxide while keeping a steady generation of electricity [1]. In current light water reactors, zircaloys have been used as a fuel cladding material mostly because of its low nuclear reaction cross section. However, the strong exothermic reaction of zircaloys with hot water and/or steam generates hydrogen while further increasing water temperature, creating a large amount of highly flammable hydrogen gas. This generation of hydrogen gas exacerbated the Fukushima inci-

***Corresponding author:** *Daniel Morrall, Graduate School of Energy Science, Kyoto University, Yoshida-honmachi, Sakyou-ku, Kyoto 606-8501; Institute of Advanced Energy, Kyoto University, Gokasho, Uji, Kyoto 611-0011, Kyoto, Japan, Tel: +81-774-38-3478*

Accepted: December 27, 2018; **Published:** December 29, 2018

ISSN 2631-5076

9 772631 507005

Morrall et al. Int J Metall Met Phys 2018, 3:026

Citation: Morrall D, Yen-Jui H, Yabuuchi K, Kimura A, Ishizaki T, et al. (2018) Corrosion Behavior of Mechanically Alloyed SUS304L with Zirconium Addition in High-Temperature Water. Int J Metall Met Phys 3:026

dent in Japan and drove a greater interest in the research on alternative cladding materials [2]. Iron-based stainless steels have been proposed as one alternative cladding material due to having several desirable characteristics: 1) High corrosion resistance, 2) Phase stability at high temperatures, 3) No α′ embrittlement that can plague ferritic/martensitic (F/M) steels under radiation [3]. A second alternative for protecting cladding materials is to add a thin barrier coating to protect direct corrosion reaction with zirconium. However, the coating has the issue of small cracks leading to a significant corrosion of the zirconium substrate. Austenitic stainless steels carry with them their own set of issues, ie. the well-known critical issues of stress corrosion cracking (SCC) and void swelling at relatively low dpa [4-6].

The materials for use in advanced nuclear system applications would need to have sufficiently high strength at high temperatures, high corrosion resistance, and a high degree of radiation tolerance. Currently much research has been completed on F/M steels with the addition of nano-sized oxides, which have been shown to improve several characteristics of F/M steels such as radiation tolerances and yield strength through several mechanisms [7-9]. Especially, one of the authors of this work developed 15Cr-5Al-oxide dispersion strengthened (ODS) ferritic steels added with small amount of zirconium which showed a significant strengthening of Al-added ODS steels, which was due to the alteration of the lower number density of coarse (Y, Al) oxides with a higher number density of fine (Y, Zr) oxides [10-16].

In our previous work, we reported the improvements in mechanical properties of 304L stainless steel by the addition of a small amount of high purity zirconium, as an oversized element, where a rather high yield strength of 767 MPa and a significantly reduced grain size of 0.42 μm were achieved [17]. This very fine grain size is attributed with being the primary factor for the high yield strength. Additionally, the high purity zirconium resulted in the formation of thermodynamically stable ZrO_2 particles further enhancing the mechanical properties and reducing the possibility of ZrO_2 forming upon exposure to high temperature steam [18]. It should be noticed that a small amount of zirconium addition less than 1 at. % can be neglected as an accelerator for oxidizing corrosion reaction heat with steam.

Improving the corrosion resistance of structural materials is one of the most studied areas of nuclear materials engineering. As such, there have been many reports on the corrosion behavior of various types of stainless steels and other alloys in a wide variety of corrosive environments. Grain size was typically found to have an impact on corrosion behavior. Li, et al. performed corrosion testing of ODS 304 steel with a reported grain size around 500 nm in supercritical water at 600 °C/25 MPa for 1000 hours [19]. They reported an improved corrosion resistance in the ODS austenitic steel compared to non-ODS austenitic steels and attributed this improvement to a combination of reduced grain size and the presence of nano-sized oxide particles hindering cation diffusion [19]. A grain size effect on corrosion properties in other alloys and corrosive environments has also been reported. Wang, et al. reported on the effects of grain refinement in Ni-Cr alloys in molten salt (Li, Na, K)F and found that a fine-grained alloy resulted in greater weight loss that also increased with increasing chromium content, meaning a reduced corrosion resistance [20]. Conversely, J. Lv, et al. reported on the effects of grain size on the corrosion resistance of Ni-based alloy 690 in a borate buffer solution at 300 °C that grain refinement enhanced the formation of a Cr_2O_3 layer and improved corrosion resistance properties [21]. It would seem then that the grain size effects on corrosion behavior can vary between alloys and corrosive environments. In addition to the grain size, S. Gollapudi reported that nanocrystalline materials exhibited faster passivation kinetics and an increase the formation of a passive layer to improve corrosion resistance [22].

The corrosion resistance of stainless steels have been widely studied in water under widely varying conditions. Gui, et al. studied the temperature dependence of corrosion resistance in SUS304 in a range of temperatures from 25 °C to 450 °C with both coarse grains and nanocrystalline grains [23]. They concluded that above 300 °C the chromium oxide passivation layer becomes comparatively thin due to an enhancement of chromium diffusion along grain boundaries [23]. Several researchers have investigated corrosion properties of SUS304 in supercritical water (SCW) and reported that the SUS304 exhibited no significant susceptibility to corrosion or stress corrosion cracking (SCC) in SCW when the average grain size was small and/or when nanoparticles existed [19,24,25].

As for the effects of zirconium addition on the corrosion properties in austenitic stainless steels, it was reported that a small addition of zirconium suppresses the formation of a Cr-depleted zone along grain boundaries under ion irradiation [26]. In this study, we compare corrosion behavior between mechanically alloyed MA304LZ, which has a small amount of zirconium addition with an average grain size of 0.42 µm, and conventional SUS304L to understand the effects of zirconium addition and grain size on the corrosion behavior of SUS304L austenitic stainless steel.

Experimental

Materials

The tested austenitic stainless steel (MA304LZ) was produced from pre-alloyed SUS304L powder and high purity (99.9%) zirconium powder (suspended in water) at 0.7 wt.%. The mixed powder was obtained by milling in a P-5 Fritsch planetary ball mill at 200 rpm for 48 hours in an argon environment with a ball-to-powder ratio of 9:10 in weight. Both the milling balls and milling chamber were composed of SUS304 stainless steel. A rather low ball-to-powder ratio along with low rotation speed was used to alleviate the affixing issue of the resulting powder to the mixing pot which has been encountered by previous researchers [3,27]. The milled powder was encapsulated in a steel tube and evacuated to 1×10^{-3} Pa for degassing. Then consolidated through hot isostatic pressing (HIP) at 140 MPa after heating to 950 °C at a heating rate of 300 °C/h. The consolidated bulk material was annealed in argon gas at 1000 °C for 30 min followed by quenching into water at ambient temperature. The chemical compositions are the same as our previous work and are listed in Table 1 [17].

Corrosion tests

Coupon-type specimens of MA304LZ and SUS304L were cut from bulk materials and polished from 200 grit SiC polishing foil up to 0.25 µm diamond spray. Two samples of each material were placed in two separate autoclaves at 300 °C and 500 °C, respectively, within the same supercritical water loop at 25 MPa and 8 ppm dissolved oxygen, as depicted in Figure 1. A high-pressure pump drove water into a pre-heater, two autoclaves,

Table 1: Chemical compositions of MA304LZ and SUS304L.

wt %	C	Si	Mn	P	S	Cr	Ni	Zr	O	N	Fe
MA304LZ	0.02	0.98	0.15	0.018	0.001	19.5	11.18	0.7	0.018	0.074	Bal
SUS304L	0.03	0.59	0.99	0.031	0.002	18.4	9.71	-	0.004	0.051	Bal

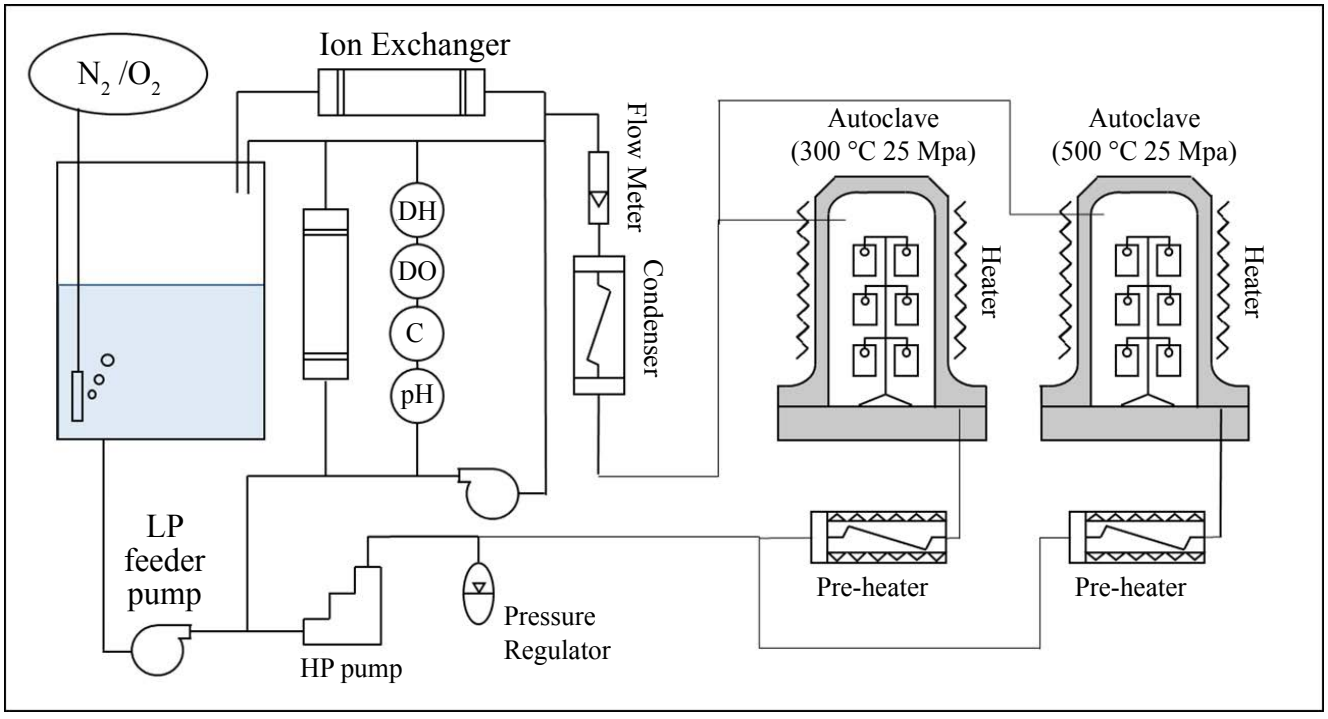

Figure 1: Corrosion test loop in high temperature water (300 °C/25 MPa) and supercritical water (500 °C/25 MPa).

heat-exchanger, and ion-exchanger and back to a water tank. A condenser dumped residual heat to an external chiller. High purity oxygen and nitrogen were injected into the water tank to control dissolved-oxygen. The samples were removed and replaced at 100, 300, 600 and 1000 hr for weight gain measurements.

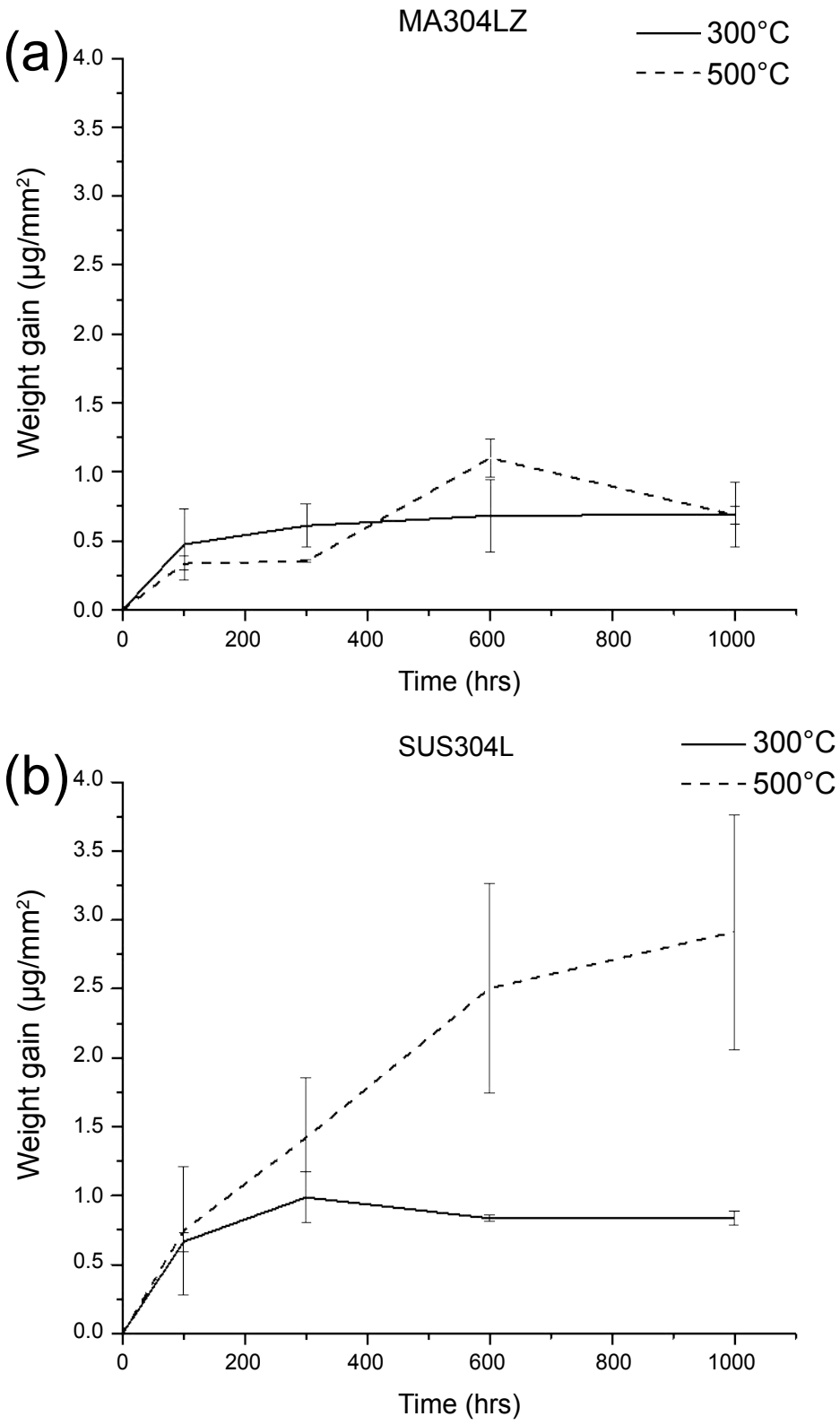

Figure 2: Weight gains of a) MA304LZ; and b) SUS304L after corrosion tests up to 1000 hr in high temperature hot water (300 °C, 25 MPa) and SCW (500 °C, 25 MPa).

Chemical analysis of corrosion layer

For the observation of corrosion layer, cross sectional areas of MA304LZ and SUS304L were mechanically polished up to 0.25 µm diamond powder spray for analysis using electron probe microanalysis (EPMA) and election dispersion spectroscopy (EDS). EPMA was conducted utilizing a JEOL JXA-8500F EPMA scanning electron microscope (SEM) and EDS was conducted using a ZEISS ultra 55 Field Emission (FE)-SEM.

Electrochemical Potentiodynamic Reactivation (EPR)

Three samples each of MA304LZ and SUS304L were prepared for electrochemical potentiokinetic reactivation (EPR) testing [28]. The degree of sensitization (DOS) was calculated as the ratio of i_r, the peak reactivation intensity to i_a, the peak activation current density. Three heating conditions were chosen, AR: As-received condition, SEN: Sensitized at 600 °C for 24 hr, AN + SEN: Solution annealed at 1050 °C for 1 hr followed by water quenching and sensitized at 600 °C for 24 hr. Each specimen was polished with SiC foils in increasing grit from 120 grit to 2000 grit followed by diamond powder spray polishing from 6 µm to 1/4 µm. Samples were mounted in an EPR testing chamber with a surface testing area of roughly 1 cm^2. The used electrolyte was 0.5M - H_2SO_4 + 0.01M - KSCN in a chamber that was submersed in a water bath kept at 30 °C. The electrodes used were an Ag/AgCl reference electrode and a Pt working electrode. A voltage was applied starting at roughly - 300 mV up to + 300 mV and back down to - 300 mV at a scan rate of 100 mV/min.

Results and Discussion

Weight gain measurement

Figure 2 shows the weight gains of a) MA304LZ and b) SUS304L after corrosion tests up to 1000 hr in high temperature hot water (300 °C, 25 MPa) and SCW (500 °C, 25 MPa). The weight gain of SUS304L significantly depends on test temperature, that is, it significantly increases with increasing temperature from 300 °C to 500 °C. In contrast, almost no change is observed in MA304LZ, suggesting that MA304LZ is more resistant to corrosion in SCW than SUS304L irrespective of the similar alloy compositions of

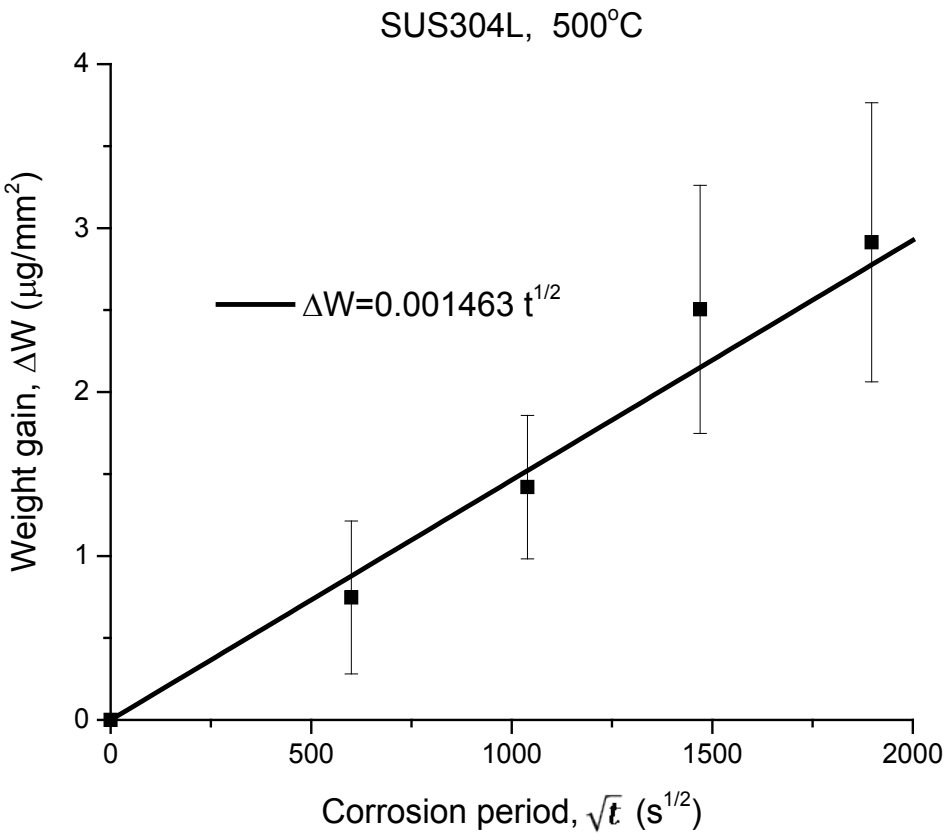

Figure 3: The ΔW - $t^{1/2}$ relation of SUS304L at 500 °C and 25 MPA (SCW). The least squares fit equation, $\Delta W = at^{1/2}$ where $a = 1.463 \times 10^{-3}$[µg/mm² • $s^{1/2}$].

chromium and nickel. It is well known that the corrosion reaction rate is controlled by diffusivity of alloy elements involved in the corrosion reactions and the corrosion rate is often expressed by the equation showing a linear relationship between the weight gain, ΔW, and the square root of test period, $t^{1/2}$. Figure 3 shows the ΔW - $t^{1/2}$ relationship of SUS304L with a linear equation. A least squares method gives the equation, $\Delta W = a\, t^{1/2}$ for the test in supercritical pressurized water at 500 °C and 25 MPa, where $a = 1.463 \times 10^{-3}$ [μg/mm^2 • s$^{1/2}$].

Chemical analysis of corrosion layer

Figure 4 shows the EPMA mapping of chemical compositions on the cross section of the tested materials at 500 °C. It is clear that chromium and oxygen coexist on the specimen surface forming chromia during corrosion tests. In contrast, no chromium carbides appear to form during the tests. At 300 °C, a similar trend was observed in

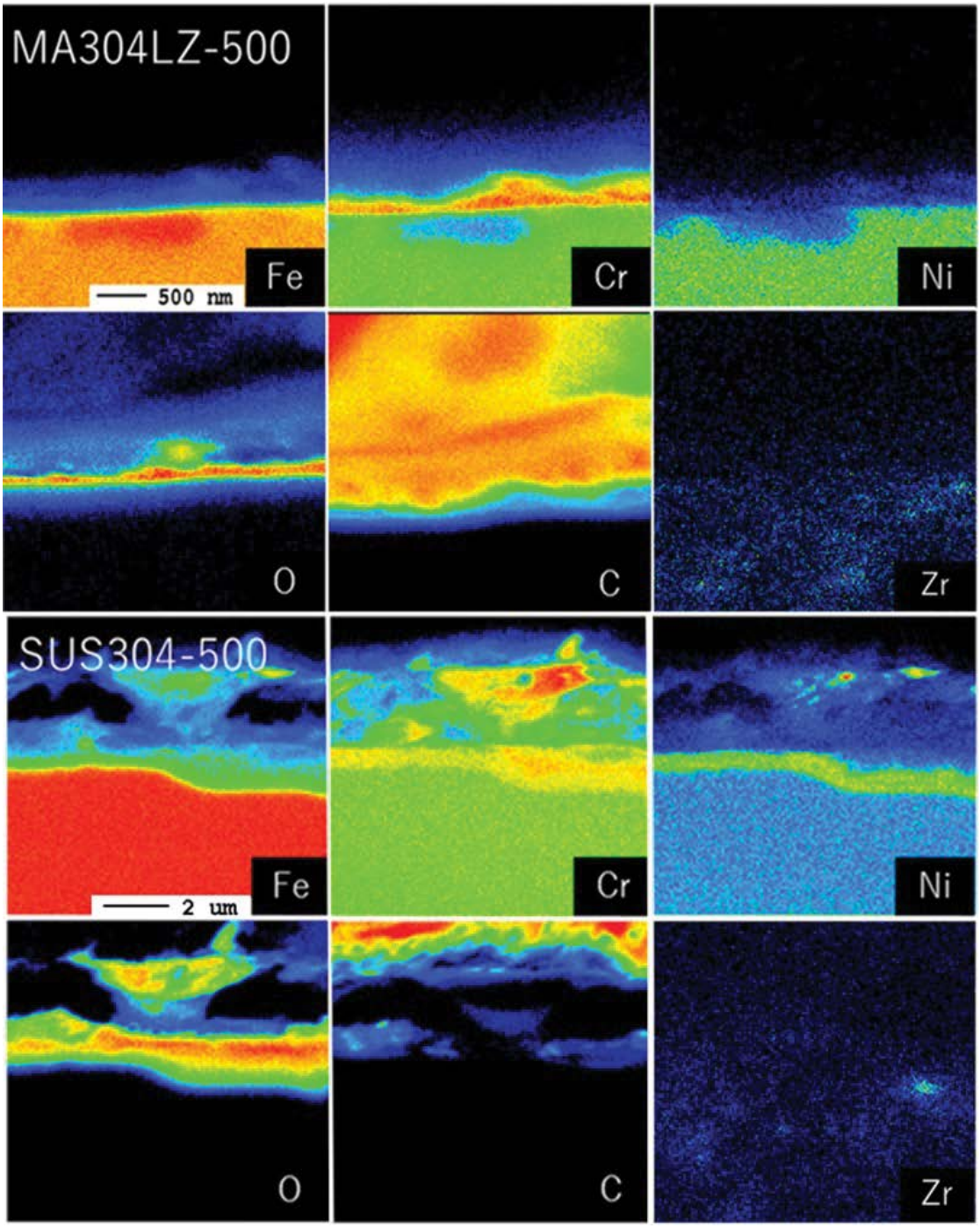

Figure 4: EPMA element mapping of chemical compositions on the cross section of MA304LZ and SUS304L at 500 °C (note the change in scale for both the materials).

Citation: Morrall D, Yen-Jui H, Yabuuchi K, Kimura A, Ishizaki T, et al. (2018) Corrosion Behavior of Mechanically Alloyed SUS304L with Zirconium Addition in High-Temperature Water. Int J Metall Met Phys 3:026

Table 2: Calculated diffusion distances after 1000 hours for Cr, Ni, and Fe in 17Cr-12Ni austenitic steel and the average oxide layer thickness obtained from EPMA line profiles of MA304LZ and SUS304L at 300 °C and 500 °C.

Test temp.	Diffusion distance (μm)						Oxide layer thickness (μm)	
	Lattice diffusion, $D_{(L)}$			Grain boundary diffusion, $D_{(GB)}$				
	Cr	Ni	Fe	Cr	Ni	Fe	MA304LZ	SUS304L
300 °C	9.0×10^{-6}	8.9×10^{-4}	3.1×10^{-6}	2.6	5.7	0.75	0.73 ± 0.08	0.45 ± 0.02
500 °C	1.2×10^{-2}	8.1×10^{-1}	6.0×10^{-3}	160	220	91	0.40 ± 0.02	1.90 ± 0.21

both steels with that observed in MA304LZ at 500 °C. As shown in Figure 2, the weight gain results at 500 °C indicated a significant difference in corrosion behavior between the two steels, and the oxide layer on the surface of MA304LZ is much thinner than SUS304L as expected. It is noticed that the nickel content in the oxidation layer of MA304LZ is reduced, while that of SUS304L is increased in comparison to the composition in the matrix. In water with dissolved oxygen, nickel is more noble than iron or chromium according to potential-pH diagrams and the disappearance of the metastable NiO and the formation of a thinner Cr_2O_3 agrees with the potential-pH diagrams [29,30]. Meanwhile, the corrosion rate is well known to be related to the atomic diffusion process as shown in Figure 3 where the weight gain is proportional to the root of the corrosion period. As for the diffusivity in a 17Cr - 12Ni austenitic stainless steel, nickel has much larger diffusivity than chromium and iron as shown in Table 2 in both the cases of lattice diffusion and grain boundary diffusion [30,31]. As for the diffusion of zirconium in austenitic stainless steels, Patil, et al. preformed tracer diffusion tests and found that zirconium should be considered a fast diffusor in 316 stainless steel with a much higher diffusivity than chromium, nickel, or iron [32].

There might be two mechanisms for the interpretation of the absence of nickel oxide in MA304LZ after the test at 500 °C: 1) The grain size

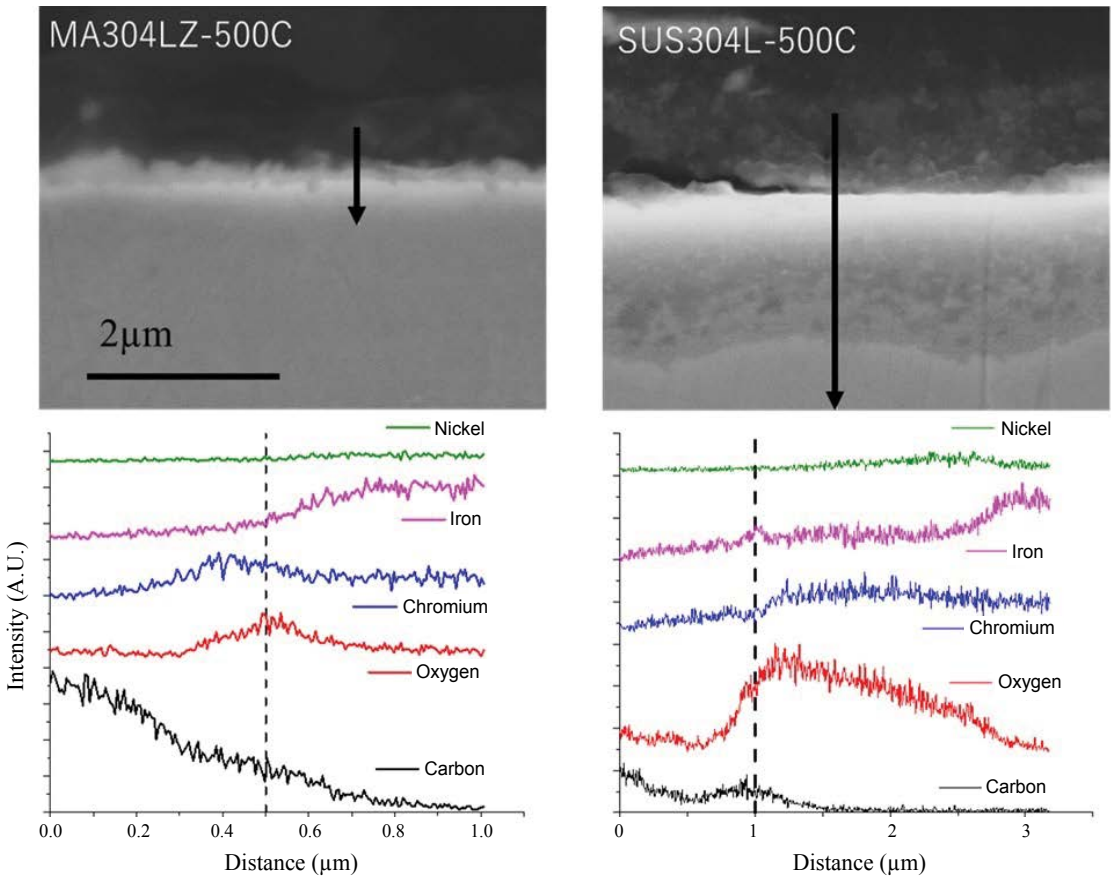

Figure 5: EDX line profiles of MA304LZ and SUS304L. Scan starting from polyfast carbon based mount across metal surface (dashed line) into metal interior.

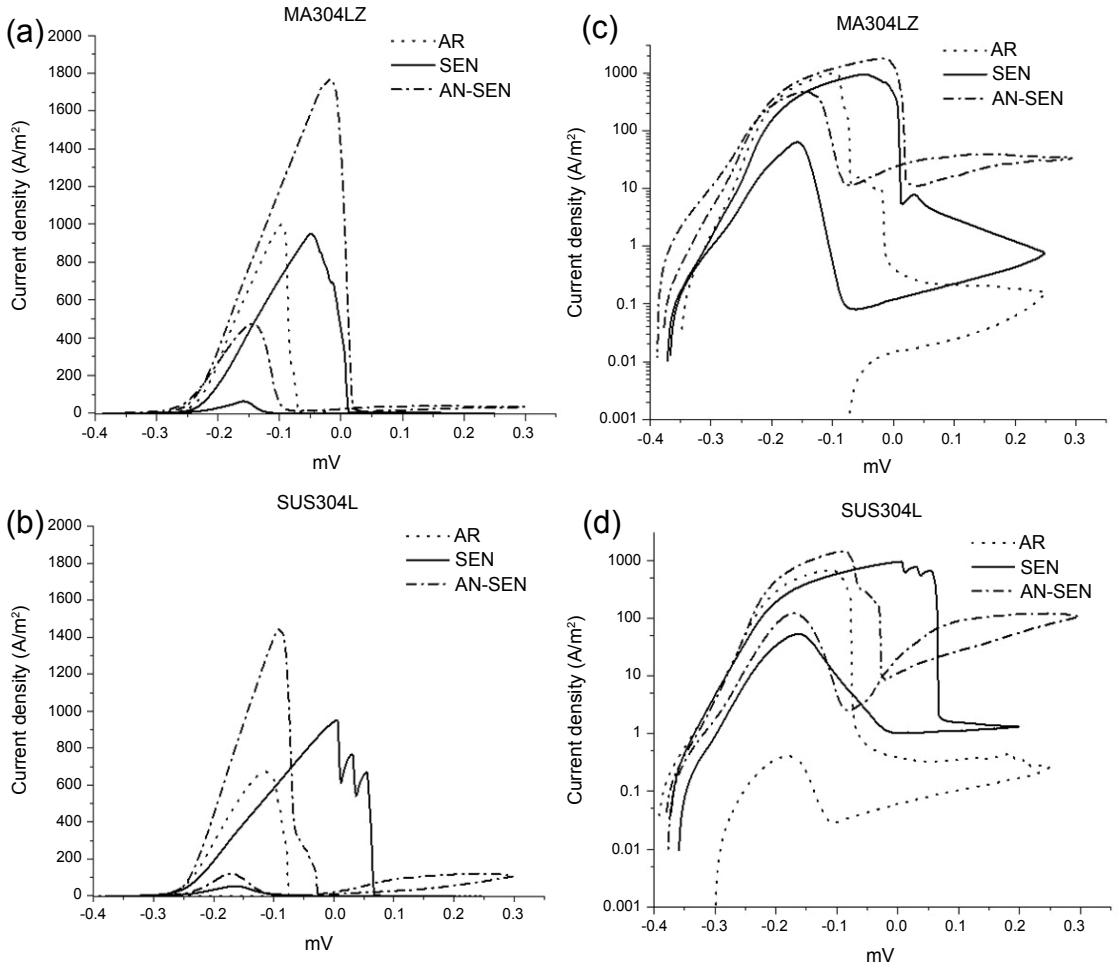

Figure 6: EPR results of a/c) MA304LZ; and b/d) SUS304L after various heat treatments: AR: As-received condition, SEN: Sensitized at 600 °C for 24 hr, AN + SEN: Solution annealed at 1050 °C for 1 hr followed by water quenching and sensitization at 600 °C for 24 hr. a/b) linear scale; and c/d) log scale of current density.

effect and 2) The zirconium effect. As for the grain size effect, grain boundaries often provide a diffusion path with large diffusivity. It is expected that MA304LZ with smaller grain size and increased grain boundary area enhances grain boundary diffusion of chromium to form a protective oxide layer. At 300 °C the diffusivities of the alloy elements are very low, but a thin chromium oxide layer was formed through the grain boundary diffusion of chromium to protect further corrosion of the steel. At 500 °C, however, in SUS304L a sufficient amount of iron can now diffuse to enhance corrosion and the corrosion proceeds following the parabolic rule as shown in Figure 3. The grain boundary diffusivity ratio of Fe/Cr is 0.57 at 500 °C and 0.29 at 300 °C, indicating that iron diffusivity becomes larger with increasing temperature in comparison to chromium. In MA304LZ with much smaller grains, however, the weight gain was actually significantly suppressed, which indicates that the formation of protective chromium oxide layer is still maintained even at 500 °C by supplying enough chromium to the surface.

As for the effect of zirconium addition, the absence of nickel oxides in MA304LZ can be also attributed to the retardation of diffusion of nickel to the surface caused by the presence of zirconium probably because the Ni-Zr bonding is much stronger than Cr-Zr and Fe-Zr bonding and may reduce the interaction with vacancies to increase the barrier to outward cationic diffusion [24]. Zirconium also has a strong affinity for oxygen and will quickly form ZrO_2. The greater affinity of zirconium for oxygen and the large diffusivity of oxygen in austenitic steels suggests that zirconium will quickly encounter oxygen and quickly be bound thereby zirconium traps oxygen and halts the diffusion of both Zr and oxygen suppressing the corrosion of iron.

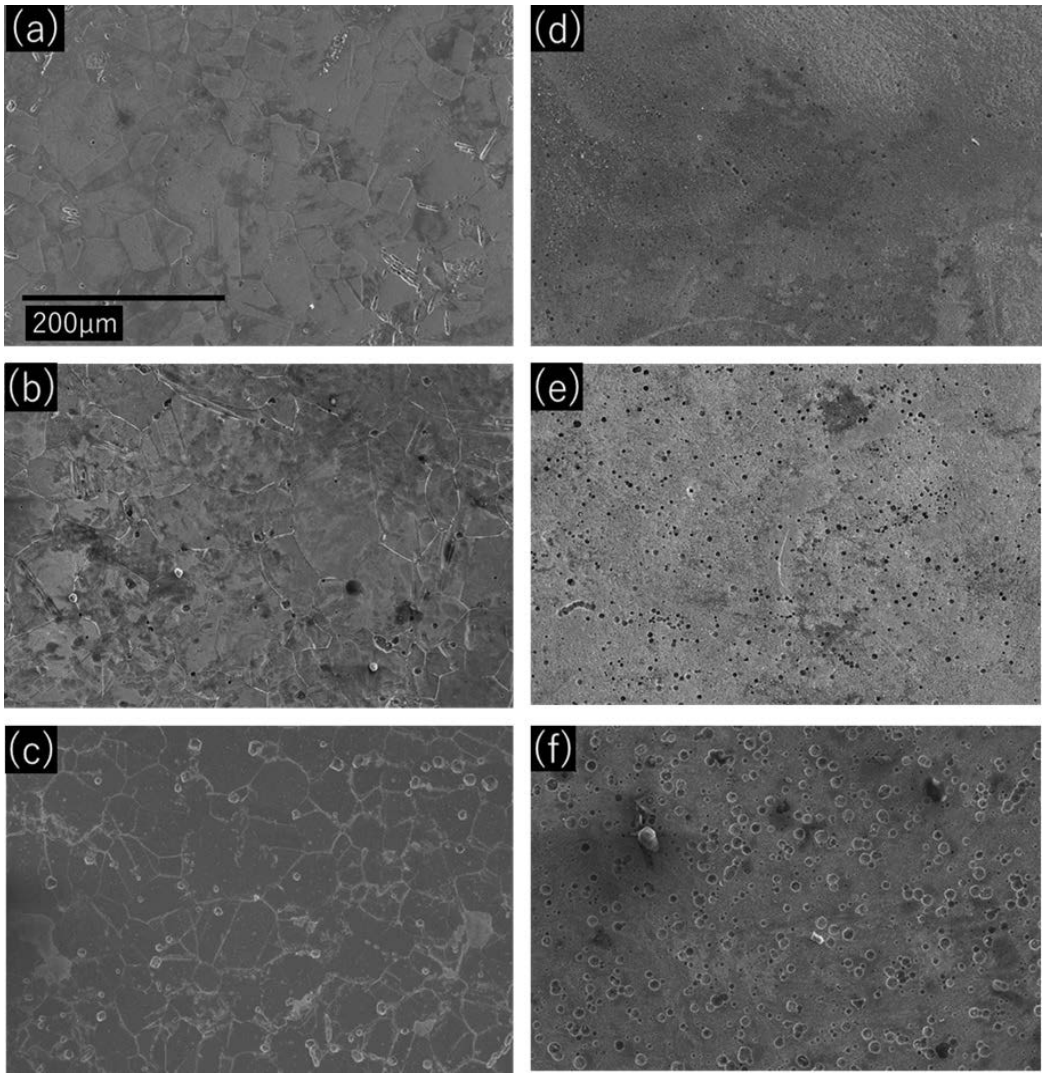

Figure 7: Surface conditions after EPR testing a) SUS304L - AR; b) SUS304L - SEN; c) SUS304L - AN + SEN; d) MA304LZ - AR; e) MA304LZ - SEN; f) MA304LZ - AN + SEN.

Table 3: EPR peak current densities and degree of sensitization (DOS) for MA304LZ and SUS304L under three conditions, AR: As received condition, SEN: Sensitized at 600 °C for 24 hr, AN-SEN: Annealed at 1000 °C and sensitized at 600 °C for 24 hr.

	MA304LZ			SUS304L		
	AR	**SEN**	**AN-SEN**	**AR**	**SEN**	**AN-SEN**
i_a (A/m²)	1000	949	1770	673	951	1450
i_r (A/m²)	-	63	473	-	53.3	120
DOS	0%	6.6%	26.7%	0%	5.6%	8.3%

Figure 5 shows the SEM cross sectional views of both steels and line profiles of each element after corrosion tests at 500 °C, showing that a much thicker (~2 µm) Cr-oxide layer was formed in SUS304L than in MA304LZ. The average oxide layer thicknesses were calculated and shown in Table 2, indicating that the oxide film thickness of MA304LZ at 500 °C is about 0.4 µm, which is comparable with those of both steels tested at 300 °C. The line profiles of chromium and oxygen are very similar, which indicates a protective chromium oxide layer is formed.

Degree of sensitization

Figure 6 shows characteristic loops of EPR curves and the estimated DOS values are shown in Table 3 for both steels, indicating that the DOS of the sensitized specimen (SEN) of each steel is

not significantly increased in comparison to that of the as-received condition. It can be said that both steels are not so sensitized by the present sensitization treatment because of the low carbon stainless steel as also reported by other researchers [33,34]. The photos of specimen surfaces after the test are shown in Figure 7. The SEN specimen of SUS304L indicates that the sensitization results in a small amount of grain boundary corrosion, while a number of small etch pits are observed in MA304LZ. An interesting feature was observed for the AN + SEN specimens after solution annealing at 1050 °C for 1 hr followed by water quenching and sensitized at 600 °C for 24 hr. The DOS of MA304LZ increased drastically from ~0 to 26.7%, while in SUS304L the DOS only increased to 8.3% under the same conditions. It is evident that the dissolution mainly occurred not along grain boundaries but at etch pits, which become much larger after this treatment. Thus, heating of MA304LZ up to 1050 °C not only coarsened the grain structure but changed the features of the carbide distribution morphology. Thus, recrystallization by the annealing process diminished the grain size effect that improved corrosion resistance of MA304LZ in SCW.

Conclusions

A mechanically alloyed austenitic stainless steel (MA304LZ) was produced from pre-alloyed SUS304L powder with a small amount of zirconium addition. The MA304LZ exhibited reduced grain size and increased tensile strength, as previously reported. In this study we examined the corrosion characteristics of MA304LZ in hot water at 300 °C/25 MPa and supercritical water at 500 °C/25 MPa. The obtained main results are as follows:

1) MA304LZ is significantly less susceptible to corrosion weight gain in SCW (500 °C and 25 MPa) than SUS304L which follows the parabolic rule between the weight gain and elapsing time.

2) The reduction of weight gain in MA304LZ can be attributed to much smaller grains which enhance the chromium diffusion through grain boundaries and consequently accelerate the formation of a protective chromium oxide layer.

3) Nickel oxides were observed in SUS304L but not in MA304LZ after the test at 500 °C. It is considered that zirconium addition suppresses nickel diffusion as well as oxygen diffusion because of the strong interaction of zirconium/nickel and zirconium/oxygen.

4) EPR measurements of DOS of annealed and non-annealed samples indicates that both steels were resistant to being sensitized to grain boundary corrosion. However, the annealing of MA304LZ at 1050 °C diminishes the beneficial grain size effect of MA304LZ.

Acknowledgements

The authors would like to express gratitude to the Japanese Ministry of Education, Culture, Sports, Science and Technology (MEXT) for their financial support. Also, gratitude is extended towards the Hitachi Corporation for contribution of the MA304LZ material for study.

References

1. SJ Zinkle, GS Was (2013) Materials challenges in nuclear energy. Acta Materialia 61: 735-758.
2. S Dryepondt, KA Unocic, DT Hoelzer, BA Pint (2015) Advanced ODS FeCrAl alloys for accident-tolerant fuel cladding. 2015 TMS Annual Meeting & Exhibition, Florida.
3. Y Miao, K Mo, Z Zhou, X Liu, K Lan, et al. (2016) Size-dependent characteristics of ultra-fine oxygen-enriched nanoparticles in austenitic steels. Journal Nuclear Materials 480: 195-201.
4. C Sun, FA Garner, L Shao, X Zhang, SA Maloy (2017) Influence of injected interstitials on the void swelling in two structural variants of 304L stainless steel induced by self-ion irradiation at 500. Nuclear Instruments and methods in Physics Research B 409: 323-327.
5. PL Maziasz, JT Busby (2012) Properties of austenitic steels for nuclear reactors applications. Comprehensive Nuclear Materials 2: 267-283.
6. H Jin, E Ko, S Lim, J Kwon, C Shin (2017) Effect of irradiation temperature on microstructural changes in self-ion irradiation austenitic stainless steel. Journal of Nuclear Materials 493: 239-245.
7. K Mo, Z Zhou, Y Miao, D Yun, H Tung, et al. (2014) Synchrotron study on load partitioning between ferrite/martensite and nanoparticles of a 9Cr ODS Steel. Journal of Nuclear Materials 455: 376-381.
8. DT Hoelzer, J Bentley, MA Sokolov, MK Miller, GR Odette, et al. (2007) Influence of particle dispersions on the high-temperature strength of ferritic alloys. Journal of Nuclear Materials 367-370: 166-172.
9. RL Klueh, DS Gelles, S Jitsukawa, A Kimura, GR Odette, et al. (2002) Ferritic/martensitic steels - overview of recent results. Journal of Nuclear Materials 307-311: 455-465.

10. A Kimura, R Kasada, N Iwata, H Kishimoto, CH Zhang, et al. (2011) Development of Al added high-Cr ODS steels for fuel cladding of next generation nuclear systems. J Nucl Mater 417: 176-179.
11. A Kimura, S Ukai, M Fujiwara (2003) Development of fuel clad materials for high burn-up operation of LWR. Proc. of GENES4/ANP2003, ISBN: 4-901332-01-5, CD-ROM file (2003) 1198. International Conference on Global Environment and Advanced Nuclear Power Plants (GENES4/ANP2003), Kyoto Research Park, 9: 15-19.
12. JS Lee, A Kimura, S Ukai, M Fujiwara (2004) Effects of hydrogen on the mechanical properties of oxide dispersion strengthening steels. J Nucl Mater 329-333: 1122-1126.
13. K Yutani, R Kasada, H Kishimoto, A Kimura (2007) Irradiation hardening and microstructure evolution of ion-irradiated ODS ferritic steels. J ASTM International 4: 1-9.
14. J Isselin, R Kasada, A Kimura, T Okuda, M Inoue, et al. (2015) Effects of Zr addition on the microstructure of 14%Cr4%Al ODS ferritic steels. Materials Transactions 51: 1011-1015.
15. P Dou, A Kimura, T Okuda, M Inoue, S Ukai, et al. (2011) Polymorphic and coherency transition of Y-Al complex oxide particles with extrusion temperature in an Al-alloyed high-Cr oxide dispersion strengthened ferritic steel. Acta Materialia 59: 992-1002.
16. P Dou, A Kimura, R Kasada, T Okuda, M Inoue, et al. (2014) TEM and HRTEM study of oxide particles in an Al-alloyed high-Cr oxide dispersion strengthened steel with Zr addition. J Nucl Mater 444: 441-453.
17. D Morrall, J Gao, Z Zhang, K Yabuuchi, A Kimura, et al. (2018) Tensile properties of mechanically alloyed Zr added austenitic stainless steel. Nuclear Materials and Energy 15: 92-96.
18. D Morrall, J Gao, Z Zhang, K Yabuuchi, A Kimura, et al. (2018) Characterization of precipitates in mechanically alloyed SUS304L type steel with zirconium addition. International Journal Metallurgy and Metal Physics 3: 015.
19. SF Li, ZJ Zhou, LF Zhang, LW Zhang, HL Hu, et al. (2016) Corrosion behavior of a 304-oxide dispersion strengthened austenitic stainless steel in supercritical water. Materials and Corrosion 67: 264-270.
20. YL Wang, Q Wang, HJ Liu, CL Zeng (2016) Effect of grain refinement on the corrosion of Ni-Cr alloys in molten (Li, Na, K)F. Corrosion Science 109: 43-49.
21. J Lv (2018) Effect of grain size on mechanical property and corrosion resistance of the Ni-based alloy 690. Journal of Materials Science & technology 34: 1685-1691.
22. S Gollapudi (2012) Grain size distribution effects on the corrosion behavior of materials. Corrosion Science 62: 90-94.
23. Y Gui, XB Meng, ZJ Zheng, Y Gao (2017) Critical temperature determination of detectable Cr diffusion enhancement by nanostructure through structural evolution analysis of the oxide films at 25-450˚C on 304 stainless steel. Applied Surface Science 419: 512-521.
24. GS Was, P ampornrat, G Gupta, S Teysseyre, EA West, et al. (2007) Corrosion and stress corrosion cracking in supercritical water. Journal of Nuclear Materials 371: 176-201.
25. S Sarrade, D Féron, F Rouillard, S perrin, R Robin, et al. (2017) Overview on corrosion in supercritical fluids. The Journal of Supercritical Fluids 120: 335-344.
26. N Shigenaka, S Ono, Y Isobe, T Hashimoto, H Fujimori, et al. (1996) Effect of zirconium addition to austenitic stainless steels on suppression of radiation induced chromium segregation at grain boundaries under ion irradiation. Journal of Nuclear Science and Technology 33: 577-581.
27. GC Allen, JM Dyke, SJ Harris, A Morris (1998) A surface study of the oxidation of type 304L stainless steel at 600K in air. Oxidation of Metals 29.
28. ASTM G108-94 (2015) Standard test method for Electrochemical Reactivation (EPR) for detecting sensitization of AISI type 304 and 304L stainless steels, ASTM International, USA.
29. D Cubicciotti (1989) Equilibrium chemistry of nitrogen and potential-pH diagrams for the Fe-Cr-H2O system in bwr water. J Nucl Mater 167: 241-248.
30. D Cubicciotti (1993) Potential-pH diagrams for alloy-water systems under LWR conditions. J Nucl Mater 201: 176-183.
31. RA Perkins, RA Padgett JR, NK Tunali (1973) Tracer diffusion of 59Fe and 51Cr in Fe-17 Wt pct Cr-12 Wt pct Ni austenitic alloy. Metallurgical Transactions 4: 2535-2540.
32. RV Patil, GP Tiwari, BD Sharma (1980) Diffusion of 99Mo, 95Zr, 60Co in 316 stainless steel. Metal Science 14: 525-528.
33. MW Chase Jr (1998) NIST-JANAF Themochemical Tables. (4th edn), J Phys Chem Ref Data, Monograph 9, 1-1951.
34. PK Davies, A Navrotsky (1981) Thermodynamics of solid solution formation in NiO-MgO and NiO-ZnO. Journal of Solid State Chemistry 38: 264-276.

Citation: Morrall D, Yen-Jui H, Yabuuchi K, Kimura A, Ishizaki T, et al. (2018) Corrosion Behavior of Mechanically Alloyed SUS304L with Zirconium Addition in High-Temperature Water. Int J Metall Met Phys 3:026